**Proceedings of the ASME 2015 International Design Engineering Technical Conferences & Computers and Information in Engineering Conference**
**IDETC/CIE 2015**
**August 2-5, 2015, Massachusetts, USA**

**DETC2015-47864**

# DESIGN AND FABRICATION OF SAFE, LIGHT-WEIGHT, FLYING ROBOTS

**Yash Mulgaonkar***
GRASP Lab
University of Pennsylvania
Philadelphia, Pennsylvania, 19104
Email: yashm@seas.upenn.edu

**Terry Kientz**
GRASP Lab
University of Pennsylvania
Philadelphia, Pennsylvania, 19104
Email: tkientz@seas.upenn.edu

**Mickey Whitzer**
GRASP Lab
University of Pennsylvania
Philadelphia, Pennsylvania, 19104
Email: mwhitzer@seas.upenn.edu

**Vijay Kumar**
GRASP Lab
University of Pennsylvania
Philadelphia, Pennsylvania, 19104
Email: kumar@seas.upenn.edu

## ABSTRACT

*This work presents the design, fabrication, and testing of a novel lightweight yet sturdy cage for micro aerial vehicles. Fabricated from a polymer infused 12k carbon-fiber using a smart liquid silicone rubber (LSR) molding process, the cage weighs only 3g and is capable of sustaining impacts at speeds up to 6m/s. We also quantitatively and qualitatively characterize the rigidity and stiffness of the cage using a universal testing machine.*

*This paper subsequently describes the fabrication methodology employed for designing the cage to achieve the high strength-weight ratio. This involves 3D printing, silicon rubber molding, plaster mold rotocasting, wet layup of carbon fiber and finally autoclaving. Finally we demonstrate a 23g autonomous, pico quadrotor capable of sustaining stable flight with collisions with the environment.*

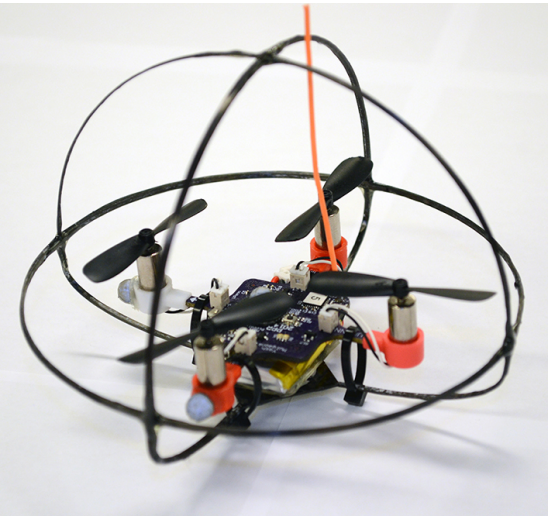

**FIGURE 1**. THE 23g PICO QUADROTOR WITH THE PROTECTIVE ROLL CAGE.

## 1 INTRODUCTION

Micro aerial vehicles (MAVs) are gathering increased interest due to their ability to fly in three dimensions and in confined spaces. However, avoiding obstacles is computationally expensive and induces delays in trajectory execution. Our aim in this paper is to develop robots that are small, extremely agile and ca-

*Address all correspondence to this author.

pable of sustaining collisions with the environment. This enables the robots to execute flight plans that leverage their agility.

This paper presents the design of a 23g pico quadrotor enclosed in a 3g protective roll cage. This robot is designed to be very nimble, fast and capable of sustaining collisions at over 4m/s. The key to our design is the multiplexed use of various components on the quadrotor and the novel fabrication techniques employed to construct the roll cage. Previous work on collision resistant robots have included projects like HyTAQ [1] and Gimball [2], both of which weigh about 400g and span more than 20cm in diameter. In contrast, in this paper we introduce the pico quadrotor capable of reaching top speeds of 6m/s within 4m and the design of an extremely lightweight yet robust protective cage weighing only 3g capable of sustaining collisions at high speeds. The substantial weight reduction in the cage was achieved by a combination of carbon composites and adopting various rapid fabrication techniques.

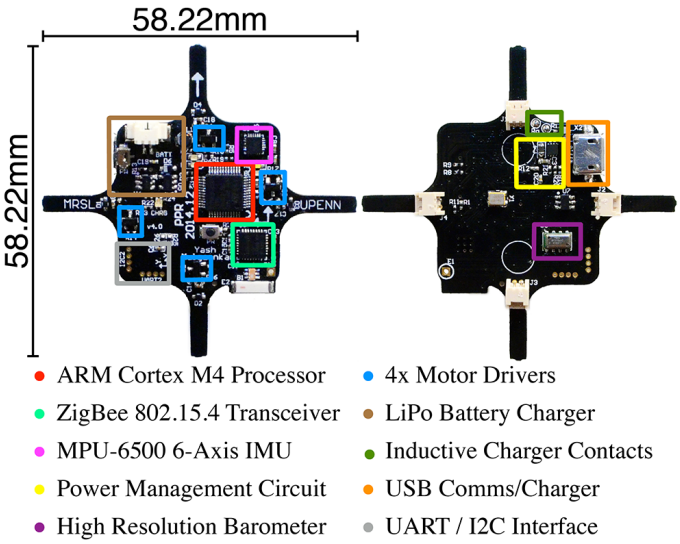


**FIGURE 2**. COMPONENTS OF THE PICO QUADROTOR AUTOPILOT

## 2 ROBOT DESIGN

### 2.1 Robot Design

Robot design and development is a very specialized field requiring a specific skill-set. A modular approach was taken when designing the pico quadrotor [3] to simplify the entire process from conception to fabrication. The hardware and software libraries were developed through an iterative process to facilitate rapid PCB redesign with minimal reproduction of supplementary code. The key innovations in the robot design center around the autopilot and the roll cage. These are described in Sections 2.2 and 3.

### 2.2 Autopilot

Quadrotor MAVs have been gaining popularity in hobbies and research applications due to the simplicity of their design and control. A wide range of these MAVs, each having very customized hardware are now readily available in the consumer market. Among the most notable autopilots are the APM 2.6 from 3D Robotics [4] and PX4's Pixhawk [5]. Both these autopilots weigh more than 35g, have very large footprints and require external motor drivers and wireless radios to control the vehicle.

Our aim for designing the pico quadrotor was to build a robot that weighed less than 50g and was less than 20cm in diameter. To fulfill these ambitious design constraints, we designed a custom autopilot, shown in Fig. 2. It comprises of nine major components. An ARM Cortex M4 STM32F303 microcontroller, interfacing with an Atmel AT86RF212 900MHz Zigbee transceiver for wireless communication, the Measurement Specialties MS5611 high resolution barometric pressure sensor for height measurement and an InvenSense MPU-6500 6-Axis MEMS inertial measurement unit. Four DC brushed motor drivers drive the motors and a power management circuit regulates power for the various components on the circuit board. An integrated battery charging circuit completes the autopilot. A USB connection to the microprocessor allows for programming and also serves as an input to the Li-Po battery charger. In addition to this, the user has access to the UART and I2C buses for external sensor interfacing.

This autopilot is made of a 1.27mm thick double layered FR4 PCB and also serves as the main structural component of the pico quadrotor. The final board is less than 34 $cm^2$ including the arms for the quadrotor and weighs less than 3g.

The pico quadrotor is powered by four DC coreless motors and carries a 3.7V, 240mAh Lithium Polymer $(LiPo)$ battery. The motors are easily attached to the autopilot with 3D printed motor mounts that snap on to the ends of each of the four arms, while the battery has specialized magnetic mounts.

### 2.3 Characterization

To study the effect of scaling on vehicle mass, the total mass of the quadrotor is divided into six categories — Battery, Cage, Motors+Propellers, Frame, Electronics, and Miscellaneous components.

Fig. 3 shows that, for the pico quadrotor, the mass contribution of the battery is about 29% while the motors contribute to a sizable 41% of the total mass. This is consistent with the fact that the thrust-weight ratio of DC brushed motors is notably decreased at smaller scales. The printed circuit board contributes about 8% to the total mass of the robot and serves the dual purpose of providing the vehicle frame. The electronics contribute a modest 6% of the total mass. The additional roll cage weighing 3g constitutes 12% to the total weight of the robot.

As expected, the mass of the vehicle decreases with its size. Also, since smaller robots have smaller motors and propellers, their moment of inertia is significantly reduced. This is in agreement with the analysis in our previous work [6]. For comparison, the AscTec Hummingbird has $I_{xx} \approx I_{yy} \approx 2.6 \times 10^{-3}$ kg m$^2$ and $I_{zz} \approx 5.0 \times 10^{-3}$ kg m$^2$, while the pico quadrotor has $I_{xx} \approx I_{yy} \approx 9.19 \times 10^{-6}$ kg m$^2$ and $I_{zz} \approx 16.01 \times 10^{-6}$ kg m$^2$.

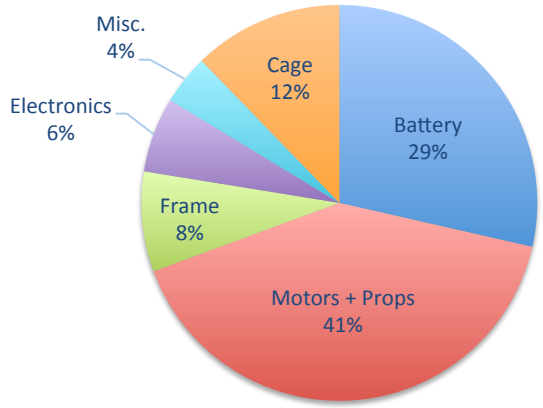


**FIGURE 3**. MASS DISTRIBUTION OF THE PICO QUADROTOR ($m$ = 0.023kg)

## 3 LIGHT-WEIGHT EXOSKELETON

### 3.1 Design

To increase the robot's resilience to collisions, we designed and manufactured a protective carbon fiber frame which is rigid and light-weight. We chose a vertical cross-section with multiple radii of curvature to reduce adverse aerodynamic effects [7] on impact.

Fig. 4 shows the free body diagram of the caged pico quadrotor during a typical collision. The forces acting on the quadrotor are its weight $m$ and total thrust $F_T$. On impact, the wall exerts a reactive force $R$ on the robot-cage system having horizontal and vertical components $R_{WH}$ and $R_{WV}$ respectively.

The overall structure of the roll cage is based on a the Gömböc [8] [9] – a homogeneous mono-monostatic object which at rest, has just one stable and one unstable point of equilibrium. Owing to this uniquely contoured structure of the cage, the center of mass (◔) of the system always lies above the point of impact ensuring stability even at high incident velocities and angles. As an added advantage of the contour chosen, the robot-cage system always passively self-rights itself on impact with the ground. This is because the net moment about the contact point is counterclockwise, resulting in the robot rotating away from the wall. Of course, aerodynamic forces because of the wall complicate this analysis, but in practice the center of mass placement is critical to ensuring stability in collisions.

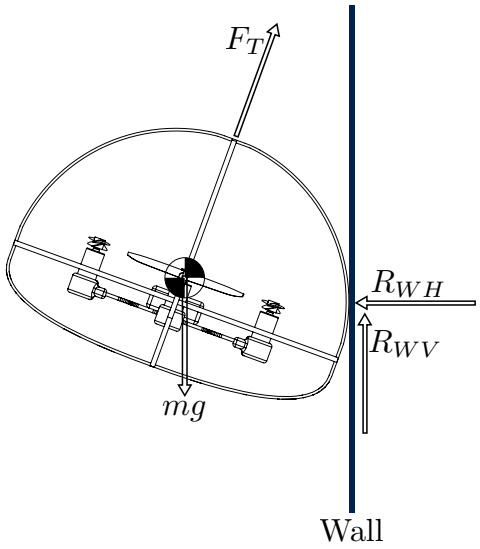


**FIGURE 4**. FREE BODY DIAGRAM OF THE QUADROTOR-CAGE SYSTEM DURING COLLISION

#### 3.1.1 Previous Prototypes

The first design iteration of the quadrotor cage consisted of ⌀1.2mm carbon fiber rods and 0.8mm thick machined carbon fiber plates. Carbon fiber hubs were used to anchor the longitudinal carbon fiber rods on the top and bottom of the cage, while aluminum splices were used to connect the lateral carbon fiber rods. A continuous carbon fiber ring around the equator of the cage provided additional structural integrity on impact. During preliminary tests, it was found that the tension in the carbon fiber rods gave the cage properties similar to that of a spring with a high spring constant.

The next design iteration involved wrapping a 3D printed mold with a thick carbon fiber tow. As the tow was wrapped around the mold, resin was placed on the tow. The carbon fiber wrapped mold was then autoclaved, following which the whole structure was placed in an acetone bath. The acetone dissolved the plastic mold, leaving only the hardened carbon fiber cage. This design method served as a proof of concept for the final cage molding technique discussed in Section 3.2. Subsequent prototypes involved substituting the plastic with a high density foam which further validated the use of carbon fiber tow for the development of extremely light-weight and stiff carbon fiber cages.

### 3.2 Fabrication of the Roll Cage

The fabrication process used to manufacture the cage is a combination of 3D printing, silicon rubber molding, plaster mold rotocasting, wet layup of carbon fiber and finally autoclaving. This multi-step process allows us to exploit the advantages of all

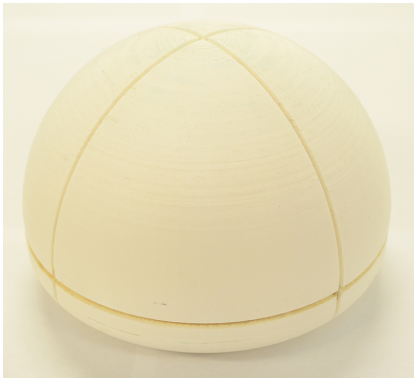

**FIGURE 5**. 3D PRINTED MOLD OF THE CAGE

the methods, resulting in an extremely rigid and lightweight roll cage. Fig.1 1 shows a cage installed on the pico quadrotor.

1. *CAD + 3D Printing*
   As a first step, we use a 3D CAD software [10] to design the desired shape of the roll cage. Next, using the same CAD tool, we create an infill of this shape to obtain the mold negative. Depending on the geometry of the cage, a suitable parting line is chosen and the mold negative is divided into two parts. Each part of the mold negative structure is then processed in an STL slicer and then 3D printed in ABS using a Fused Deposition Modeling (FDM) 3D Printer. A complete mold negative, printed with a Dimension Elite [11] 3D Printer is shown in Fig. 5.
2. *Liquid Silicon Rubber Molding*
   Each part of the 3D Printed negative is then placed in separate molding containers. Next, a carefully weighed and vacuum degassed mixture of Bluestar's V-340 silicon rubber and the CA45 catalyst is poured into these containers and allowed to cure overnight. The resulting reusable two-part silicon rubber mold is shown in Fig. 6.
3. *Plaster Rotocasting*
   Fig. 7 shows the custom built single motor rotocasting machine with a cavity of 16cm$\times$12cm$\times$16cm for creating a plaster cast in the silicon mold. The two part silicon molds are mounted in this rotocasting cavity and sealed, leaving a $\varnothing$20mm hole for pouring plaster and a $\varnothing$3mm bore for bleeding air out of the cavity.
   The cavity is then filled with a 5oz. quick-dry gypsum plaster emulsion and turned for 30 minutes, resulting in an exact replica of the 3D Printed mold negative described in step 1. This plaster cast shown in Fig. 8 now forms a hollow sacrificial negative of the roll cage.
4. *Carbon-Fiber Wet Layup*
   The penultimate step is to wrap pre-preg 12K carbon fiber reinforced polymer (CFRP) tow in the grooves of the shell and thermally cure the assembly for 3 hours at 310$^\circ$F. Finally, the plaster shell is either cracked manually or the cured assembly is dipped in water to dissolve off the plaster. Fig. 8 shows the carbon fiber tow wrapped around the plaster shell. The shell is partially cracked to emphasize the thickness of the plaster crust. The resulting cage is then mounted around the pico quadrotor and is shown in Fig 1.

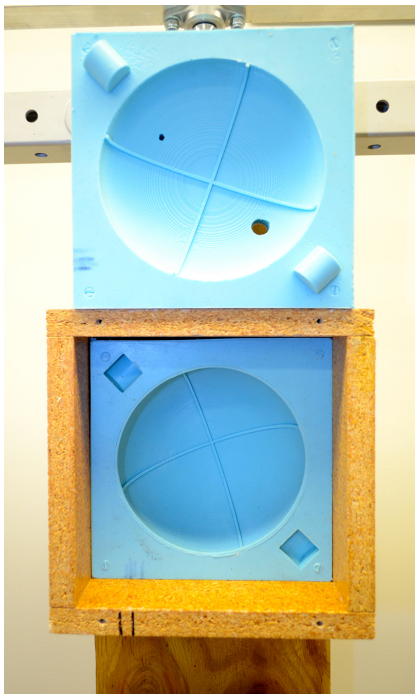

**FIGURE 6**. SILICON NEGATIVE OF THE 3D PRINTED MOLD

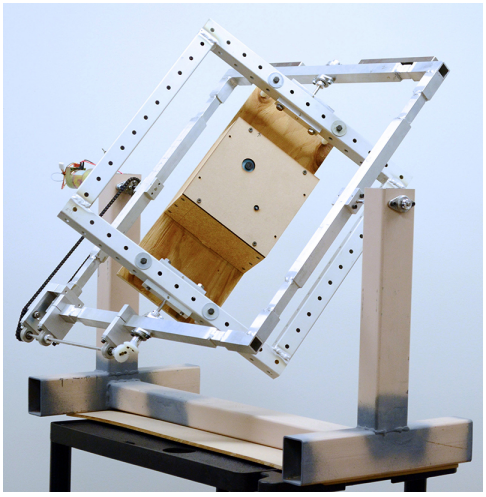

**FIGURE 7**. THE CUSTOM BUILT ROTOCASTING MACHINE

**FIGURE 8**. A PLASTER SHELL WITH CARBON FIBER TOW WRAPPED AROUND IT. THE CRACKED PORTION SHOWS THE WALL THICKNESS

## 4 EXPERIMENTAL EVALUATION

Every iteration of the cage was subject to extensive tests to ensure the feasibility of the designs to collisions with the environment. The results of the latest iteration of the roll cage to stress tests and collisions with the environment are presented in Sections 4.1 and 4.2.

### 4.1 Stress Tests

The horizontal plane of the cage was subject to compression in the MTS Criterion Model 43 universal tester to characterize the stress, strain and deformation.

The cage was secured in the compression platens and subject to a uniformly increasing load. Since carbon fiber is anisotropic, the stress is dependent on the orientation of the load. To maximize the strength of the cage, we loaded the carbon fiber longitudinally. Figures 9 shows the stress-time and strain-time curves for the cage.

The stress-strain curve for the cage is shown in Fig. 10 exhibits several discontinuities indicating the successive appearance of cracks along the CFRP. These cracks ran perpendicular to the loading direction. The first major visible crack in the cage occurred at a load of over 78N and is highlighted by the red ellipse in Fig. 10. This is much higher than the forces exerted by the cage under normal operating conditions.

### 4.2 Collisions

The robustness of the quadrotor to collisions was validated by studying impact with a wooden wall and a vertical PVC pipe. For this, we developed a dynamical model and empirically verified the results.

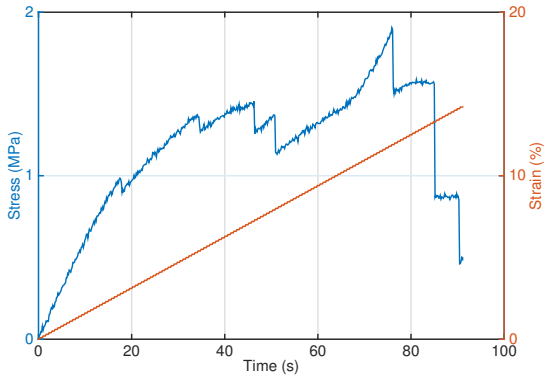


**FIGURE 9**. STRESS-TIME AND STRAIN-TIME CURVES OF THE 12K CARBON FIBER CAGE

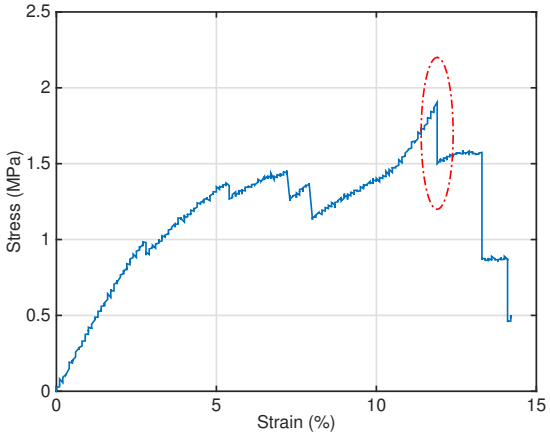


**FIGURE 10**. STRESS-STRAIN CURVE OF THE 12K CARBON FIBER CAGE

**4.2.1 Collisions With a Vertical pole** In order to better study the effect of the cage on the reflected angle, we conducted collisions against a vertical cylinder. The angle of incidence, $\theta_i$, was defined as the angle between the forward direction and the point of contact on the cage. This is illustrated in Fig. 11. The analysis of this experiment is similar to that explained later in Section 4.3. In this case, the impact plane is tangential to the cylinder surface at the point of collision, where the local normal is given by $\hat{n}$.

Several collisions at different incident angles are plotted in Fig. 12. The vehicle was commanded to move along the $X$ axis, while the $Y$ position was varied in order to generate the desired angles of incidence.

Fig. 12 shows the collisions of the pico quadrotor with the vertical PVC pole. The *coefficients of restitution* along the $X$ and $Y$ axes, $e_x$ and $e_y$ were found to be -0.5824 and 0.6686 respectively. During these experiments, we successfully recovered

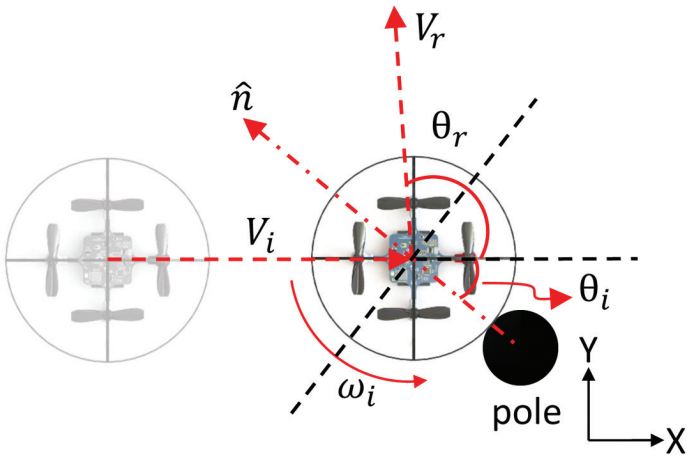


**FIGURE 11**. COORDINATE SYSTEM OF COLLISIONS WITH A VERTICAL POLE

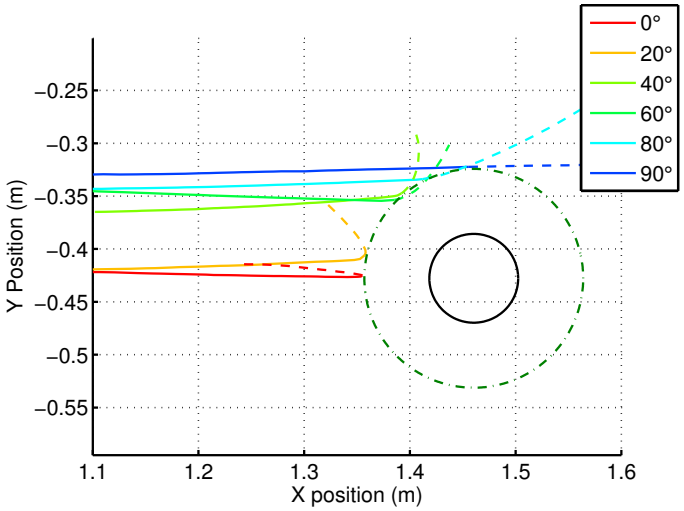


**FIGURE 12**. COLLISIONS WITH A VERTICAL POLE (BLACK) WITH IMPACTS AT VARIOUS ANGLES ALONG THE RIM OF THE CAGE. THE GREEN DOTTED CIRCLE DENOTES THE IMPACT PERIMETER

from collisions at impact velocities of 4m/s. The cage easily survived drop tests with impact velocities of 12m/s.

Frame grabs from a 800FPS high speed video displayed in Fig. 13 show the collision of the pico quadrotor with a vertical pole with and without the protective cage. Note the contrast in Figures 13(d) and 13(i). The former image shows that one of the propeller stalls on impact while the latter image shows that the cage prevents this failure mode. Figures 13(e) and 13(j) show that the cage also damps the effect of the impact on the attitude of the robot.

### 4.3 Impact Model

With these experiments, we aim to characterize how the state of the pico quadrotor is affected by collisions with the environment, while simultaneously testing the durability of the protective cage. Since the true dynamics of the vehicle-surface interaction are complex, we opt to simplify the problem by employing *Garwin's model*. [12] In this model, we experimentally determine two *coefficients of restitution*, $e_x$ and $e_y$, which empirically describe the details of the velocity transition that occurs at the moment of impact. Under ideal test conditions, $e_x = 1$ corresponds to a collision with a frictionless surface, while $e_y = 1$ models an elastic collision.

Collisions of the pico quadrotor with a vertical wall were evaluated by varying the angle of incidence, $\theta_i$, as shown in Fig. 14. The pico quadrotor is modeled as a spherical projectile, with mass $m$ and radius $R$, impacting the wall at angle $\theta_i$. The linear and angular velocities at the time of impact are $V_i$ and $\omega_i$, respectively. The purpose of this experiment is to empirically determine the coefficients of restitution $e_x$ and $e_y$.

We proceed by calculating an impact trajectory for each incident angle of interest. The vehicle is flown through the trajectory until it impacts the wall at a predetermined point. Throughout the experiment, the Vicon motion capture system records the position of the robot, as well as its linear and angular velocities $(V_{k,x}, V_{k,y}, \omega_k)$. Here, the subscripts $x, y$ denote the $X$ and $Y$ components of linear velocity while $k = i, r$ indicates either the incident or reflected phase of the trajectory.

This recorded data is used to build an impact model of the pico quadrotor and calculate the coefficients of restitution $e_x$ and $e_y$ by applying techniques similar to those in [12, 13]. Their values are determined with the following relations:

$$e_y = -\frac{V_{r,y}}{V_{i,y}} \tag{1}$$

$$e_x = -\left(\frac{V_{r,x} + R\omega_r}{V_{i,x} + R\omega_i}\right) \tag{2}$$

Here, $0 \leq e_y \leq 1$ is the perpendicular coefficient of restitution characterizing the elasticity of the cage-obstacle interaction, where $e_y = 1$ corresponds to a fully elastic collision. The tangential coefficient of restitution $-1 \leq e_x \leq 1$ models the friction between the cage and the wall during the impact.

Fig. 15 shows the actual position of the pico quadrotor colliding with the wall at different commanded incident angles. Equations 1 and 2 were employed in combination with data from the above experiments to empirically determine the values of $e_x$ and $e_y$ as -0.3400 and 0.7896, respectively.

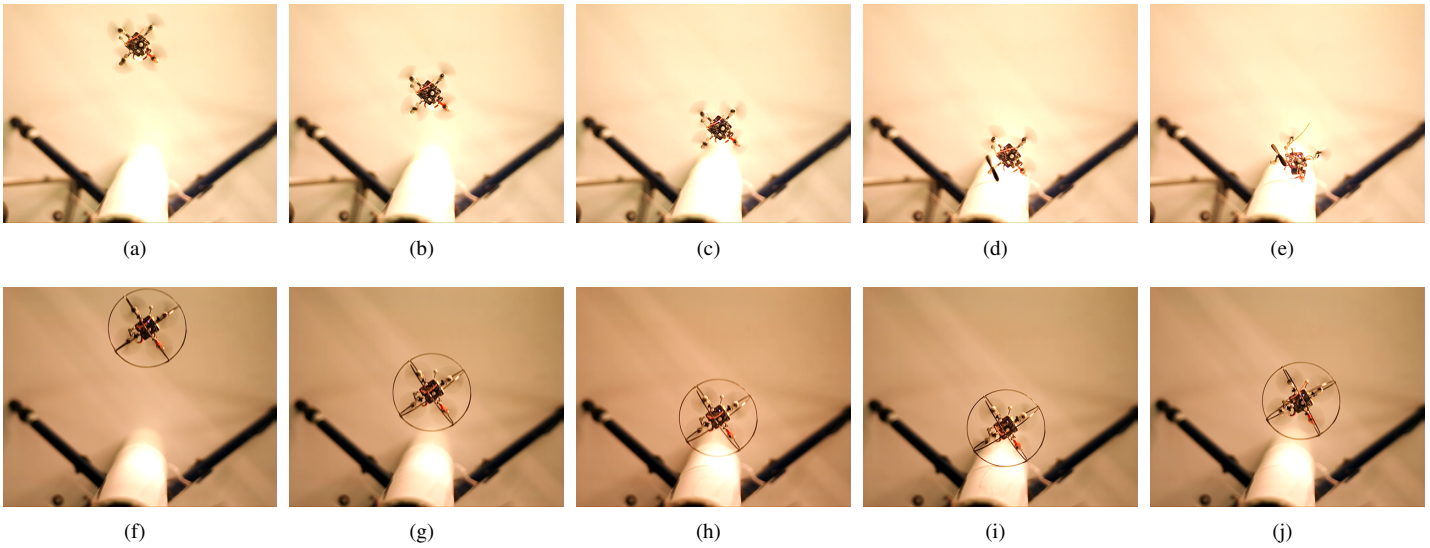


**FIGURE 13**. HIGH SPEED VIDEO FRAMES SHOWING THE COLLISION OF THE PICO QUADROTOR WITH A VERTICAL POLE WITHOUT THE CAGE (FIGS. 13(a) - 13(e)) AND WITH THE CAGE INSTALLED (FIGS. 13(f) - 13(j)).

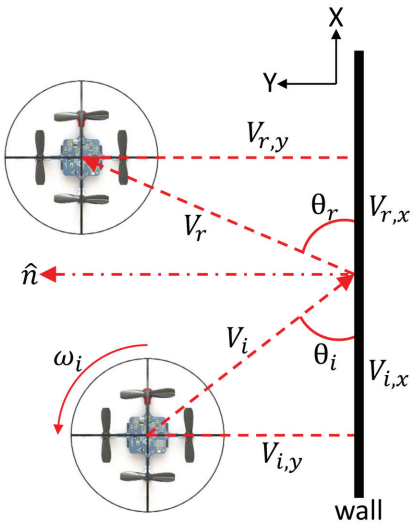


**FIGURE 14**. COORDINATE SYSTEM OF COLLISIONS WITH A VERTICAL WALL

These values of $e_x$ and $e_y$ were then used to estimate the reflected linear velocities and the reflected angle $\theta_r$ of the pico quadrotor using the following relations:

$$V_{r,x}(est) = -\frac{V_{i,x}(1+\alpha e_x)+\alpha R\omega_i(1+e_x)}{(\alpha-1)} \tag{3}$$

$$V_{r,y}(est) = -e_y V_{i,y} \tag{4}$$

$$\theta_r = tan^{-1}\left(\frac{V_{r,x}(est)}{V_{r,y}(est)}\right) \tag{5}$$

Where $\alpha$ is determined by:

$$\alpha = \frac{I}{mR^2} \tag{6}$$

Using Garwin's model, we were able to predict the reflected velocities to within $0.1^{m}/_{s}$, and the reflection angles to within 0.1554 radians.

### 4.4 Drop Tests

To further test the resilience of the roll cage to crashes and collisions, we conducted a series of drop tests from various heights. Fig. 16 shows one such test. Figures 16(c) and 16(d) show a distinct compression of the frame on impact. However, this deformation does not affect the rotation of the propellers.

The cage has proven to withstand a free-fall from a height of 8m reaching a terminal velocity of over 12m/s.

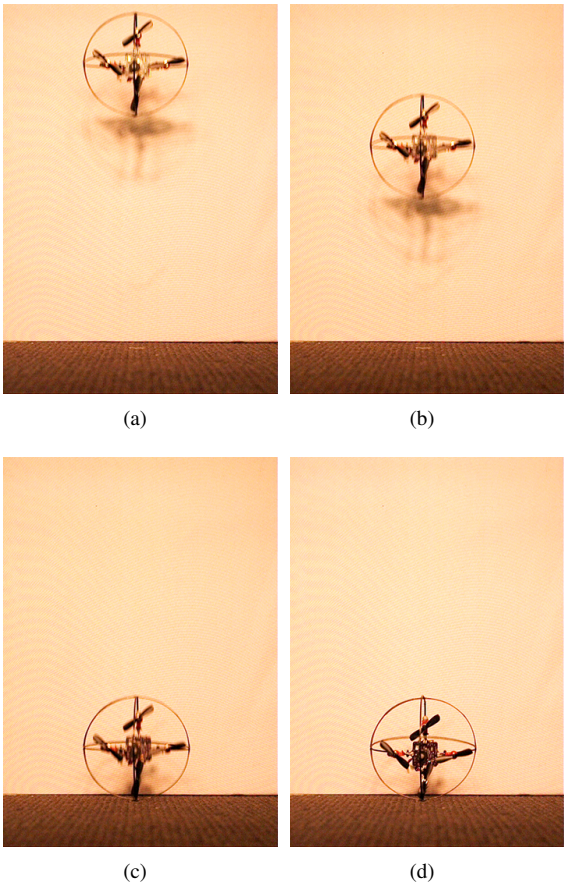


**FIGURE 16**. HIGH SPEED VIDEO FRAMES SHOWING THE FREE-FALL OF THE PICO QUADROTOR

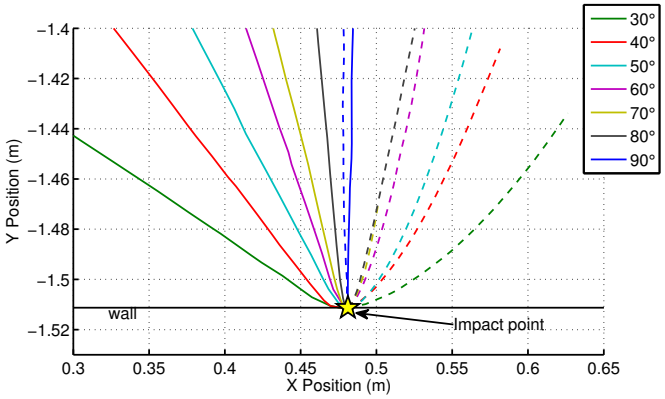


**FIGURE 15**. COLLISIONS WITH A VERTICAL WALL AT VARIOUS ANGLES OF INCIDENCE

## ACKNOWLEDGMENT

The authors gratefully acknowledge the Department of Mechanical Engineering and Applied Mechanics at the University of Pennsylvania and Prof. Bruce Kothmann for granting us access to the Mechanical and Aerodynamic Testing Lab and Sawyer Brooks for his help with conducting the stress analysis on the universal testing machine. We are also thankful for support from ARL Micro Autonomous Collaborative Technology Alliance Grant no. W911NF-08-2-0004 and NSF Grant IIS-1138847.

## REFERENCES

[1] Kalantari, A., and Spenko, M., 2013. "Design and experimental validation of hytaq, a hybrid terrestrial and aerial quadrotor". In Robotics and Automation (ICRA), 2013 IEEE International Conference on, pp. 4445–4450.

[2] Briod, A., Kornatowski, P. M., Zufferey, J.-C., and Floreano, D., 2014. "A Collision Resilient Flying Robot". *Journal of Field Robotics,* ***31***(4), pp. 469–509. in press (airburr).

[3] Mehta, A. M., Rus, D., Mohta, K., Mulgaonkar, Y., Piccoli, M., and Kumar, V., 2013. "A scripted printable quadrotor: Rapid design and fabrication of a folded mav". *16th International Symposium of Robotics Research (ISRR '13)*, Dec.

[4] 3D Robotics. `http://3drobotics.com/`.

[5] Pixhawk. `http://www.pixhawk.org/`.

[6] Mulgaonkar, Y., Whitzer, M., Morgan, B., Kroninger, C., Harrington, A. M., and Kumar, V., 2014. "Power and weight considerations in small, agile quadrotors". *Proc. SPIE,* ***9083***, pp. 90831Q–90831Q–16.

[7] Powers, C., Mellinger, D., Kushleyev, A., Kothmann, B., and Kumar, V., 2012. "Influence of aerodynamics and proximity effects in quadrotor flight". In Proceedings of the International Symposium on Experimental Robotics.

[8] Várkonyi, P., and Domokos, G., 2006. "Mono-monostatic bodies". *The Mathematical Intelligencer,* ***28***(4), pp. 34–38.

[9] Domokos, G., and Várkonyi, P. L., 2008. "Geometry and self-righting of turtles". *Proceedings of the Royal Society of London B: Biological Sciences,* ***275***(1630), pp. 11–17.

[10] SolidWorks 3D CAD software. http://www.solidworks.com/.

[11] The Dimension Elite 3D Printer. http://www.stratasys.com/3d-printers/design-series/dimension-elite.

[12] Garwin, R. L., 1969. "Kinematics of an ultraelastic rough ball". *American Journal of Physics,* ***37***, pp. 88–92.

[13] Cross, R., 2002. "Measurements of the horizontal coefficient of restitution for a superball and a tennis ball". *American Journal of Physics,* ***70***(5), pp. 482–489.